DJI S-1000 SPREADING WINGS OCTOCOPTER: DETERMINATION OF ROTOR DOWNWASH SLIPSTREAM SIZE

A Thesis Presented for the
Master of Science
Degree
The University of Tennessee, Knoxville

Jonathan Lemieux
December 2016

ABSTRACT

The DJI S-1000 Spreading Wings octocopter rotor downwash slipstream area of influence was measured in axial climb conditions and in straight level flight. These data were gathered using a simple apparatus of distributed anemometers and a custom made boom affixed to the drone. Straight level flight tests incurred autopilot oscillations that rendered the data gathering and analysis challenging. The best quality data was acquired during the axial climb flight tests. The axial climbs were conducted in calm winds. It was determined that the axial climbs under these conditions displaced the rotor slipstream 9 ± 2.5 cm to the rear of the drone. Its location at the front of the drone closely corresponded to the theoretical value. For straight level flights, the slipstream moved aft of the drone to 81 cm and 84 cm for airspeeds of $3\,\frac{m}{s}$ and $4\,\frac{m}{s}$ respectively. The measured size of individual rotor slipstreams was 15 cm smaller than the theoretical value.

TABLE OF CONTENTS

Chapter One Introduction and General Information 1
- Background 1
- Theory 2
  - Rotor Wake in Axial Climb 2
  - Effective Disk Area 5
  - Wake Boundaries in Forward flight 5
  - Airspeed 6
  - Rate of Climb 7
  - Effects of Altitude 7

Chapter Two Flight Planning 9
  - Methodology 9
  - Flight Test Plan 9
  - Aircraft Description 10
  - Instrumentation 12
  - Data Source and Instruments 14
  - Test Location 16
  - Predictions 17
  - Effects of Altitude 19

Chapter Three Flight test 20
- Flight Test Technique 20
  - Axial Climbs 20
  - Straight Level Flight 21
- Test Conditions 23
- Flight Planning 25
  - Rate of Climb 26
  - Velocity 26
  - Altitude 27
  - Axial Stability 27
  - Heading 28
  - Battery Life 28
  - Data Recording 29
- Data Extraction and Analysis 29
  - Data Extraction 29
  - Rate of Climb 30
  - True Airspeed 31
  - Vertical Airflow Velocity 31
  - Heading 32
  - Stabilization Period 32

Chapter Four Results and Discussion 35
  - Axial Climb Results 35

Straight Level Flight Results 37
Summary of Results 39
Chapter Five Conclusions and Recommendations 48
Conclusion 48
Recommendations 48
List of References 50
Appendix 52
Vita 54

LIST OF TABLES

Table 1 Data Source 15
Table 2 CoG Range During Test Flights 24
Table 3 Correlation Between Power Setting and Longitudinal Airspeed 27
Table 4 List of Software 30

LIST OF FIGURES

Figure 1 Airflow Visualization for a Helicopter in Axial Climb. 3
Figure 2 Location of Blade Tip Vortices as a Function of Advance Ratio (μ), Non-Dimensionalized Horizontal Location (x/R), Non-Dimensionalized Vertical Location (z/R). 8
Figure 3 Picture of DJI S1000. Source: DJI.com 11
Figure 4 Dimensions of the DJI S1000. Source: DJI..11
Figure 5 Digi-Sense Anemometer...13
Figure 6 Boom Assembly...13
Figure 7 Drone with boom assembly and anemometers....................................14
Figure 8 Top View of the Airfield. North Directly Up...16
Figure 9 Representation of Drone Axes...24
Figure 10 Example of Anemometer Data Plot...33
Figure 11 Anemometer Data Plot with Example of Data Editing.........................34
Figure 12 Airflow Velocities for Axial Climb...36
Figure 13 Airflow Velocities for Axial Climb, Corrected for Climb Rate 37
Figure 14 Airflow Velocities for 3 m/s Airspeed..38
Figure 15 Airflow Velocities for 4 m/s Airspeed..38
Figure 16 Airflow Velocities for Straight Level Flights at 2m/s, 3 m/s and 4m/s Airspeeds...41
Figure 17 Airflow Profile Around Drone During Axial Climb 42
Figure 18 Airflow Profile Around Drone with 3 m/s Airspeed 43
Figure 19 Airflow Profile Around Drone with 4 m/s Airspeed 44
Figure 20 Top View of Drone Slipstream in Axial Climb.....................................45
Figure 21 Top View of Drone Slipstream in 3 m/s Airspeed................................46
Figure 22 Top View of Drone Slipstream in 4 m/s Airspeed................................47
Figure 23 Weight and Balance Calculation Spreadsheet....................................53

ABBREVIATIONS AND SYMBOLS

A_∞	Area far below rotor disk
A	Area at rotor disk
ADS	Air Data System
AWOS	Automated Weather Observation System
B	Tip loss factor
BVT	Blade Tip Vortices
CoG	Center of Gravity
F	Force
ft	Foot
FDR	Flight Data Recorder
h	GPS altitude
h_d	Density altitude
kts	knots
lbs	Pound mass
m	Meter
$\dot{m}$	Mass flow
MB	Megabyte
NOAA	National Oceanographic and Atmospheric Administration
Δr	Change in radius dimension
r or R	Rotor disk radius
T	Trust
v	Velocity

V_c	Air velocity far above the rotor disk
v_i	Air velocity at rotor disk
v_{true}	True velocity
v_{wind}	Velocity of wind
w	Air velocity far below rotor disk
Std (subscript)	Standard day condition
TPP	Tip Path Plane
UAS	Unmanned Aerial System
W	Weight
W&B	Weight and Balance
x	Position on x axis
y	Position on y axis
z	Position on z axis
δ	Atmospheric pressure ratio
θ	Atmospheric temperature ratio
ρ	Air density
σ	Atmospheric density ratio
μ	Advance ratio
∞	Infinity

CHAPTER ONE
INTRODUCTION AND GENERAL INFORMATION

Background

The National Oceanographic and Atmospheric Administration (NOAA) currently uses a system of disposable balloons and sensors to gather atmospheric data such as pressure and temperature lapse rates for forecasting. In order to make data gathering more cost effective, they intend on using an Unmanned Aerial System (UAS). The UAS chosen is the DJI S1000 octocopter**.** It has been equipped with a boom at the end of which an air data sensor is affixed. However, it is not known if the drone rotor downwash slipstream, under certain flight and wind conditions, will have negative effects on the quality of the data. Through experimental flight, UTSI is helping NOAA to validate their new system by determining the size of the rotor slipstream.

NOAA plans to gather data when the UAS is in an axial climb flight profile. In order to account for wind speeds that the hovering drone might encounter, data will be collected in hover and longitudinal flight conditions.

This experiment will provide NOAA with an understanding of the influence area of the rotor downwash slipstream, and hopefully confirm the validity of their UAS apparatus concept to replace the current disposable weather balloon method.

Theory

Rotor Wake in Axial Climb

The basic laws of physics dictate that for successful heavier-than-air flight to occur, aircraft need to produce a downward force that corresponds to their own weight. Essentially, it needs to push enough air downwards to create the lift force necessary to fly. For rotary wing aircraft, this is done through the help of one or more rotors to create thrust by sucking air from above them and pushing it down below. Figure 1 is a good illustration of this phenomenon for an axial climb. The air velocity at the rotor disk, also known as the induced velocity, is represented by v_i while the air velocity far below the disk is represented by w. The disk area at infinity, ∞, will be further referred to as *vena contracta*.

Froude's approach is a widely used when analyzing hover performance. It assumes that the rotor has an infinitely thin rotor disk comprised of an infinite number of rotor blades. The blades have zero thickness and produces an asymmetric airflow all around the rotor. It can be treated as incompressible, one dimensional quasi-steady flow.

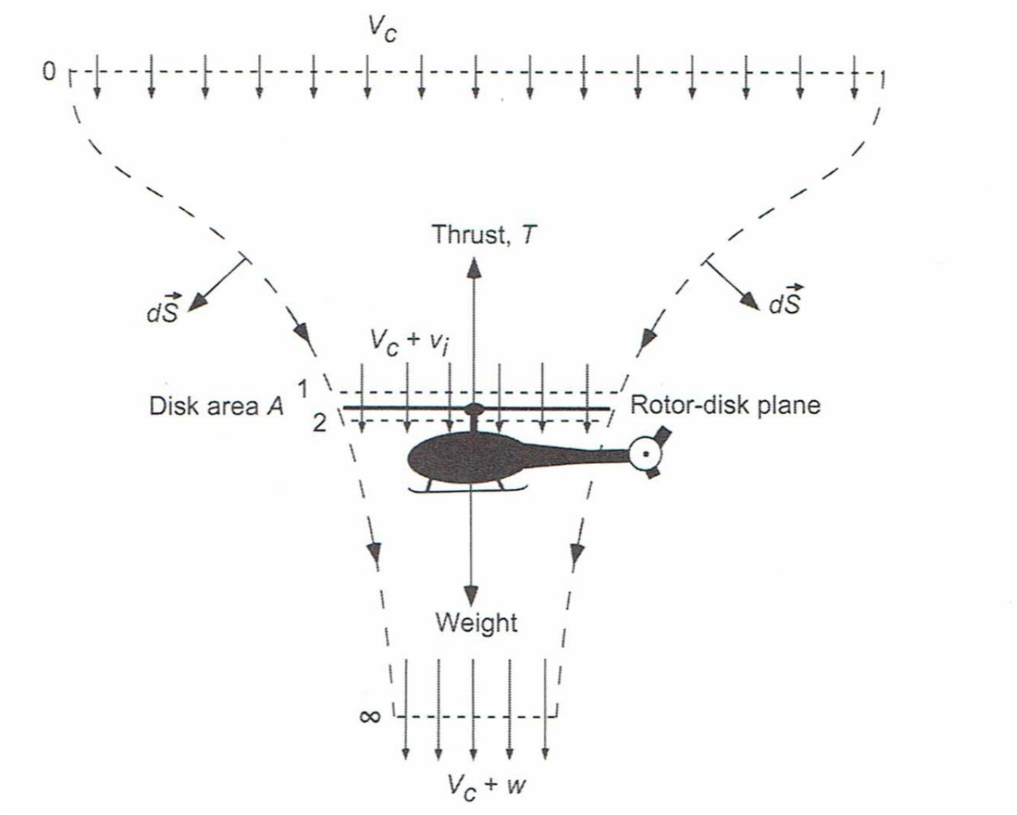

Figure 1 Airflow Visualization for a Helicopter in Axial Climb.

Figure reproduced with permission from Cambridge University Press. Source: Leishman, J.G. "Fundamentals of Rotor Aerodynamics," *Principles of Helicopter Aerodynamics*, Second Edition, Cambridge University Press, Cambridge, NY, 2006, p. 82

Based on the assumptions made by Froude, the conservation of mass with 1-D steady flow theory (1) and the rotor thrust (2) equations can be used.

$$\dot{m} = \rho A_\infty (V_c + w) = \rho A (V_c + v_i) \quad (1)$$

$$-\vec{F} = T = \dot{m}(V_c + w) - \dot{m}V_c = \dot{m}w \quad (2)$$

This implies that the work done by the rotor per unit time is

$$T(V_c + v_i) = \frac{1}{2}\dot{m}(V_c + w)^2 - \frac{1}{2}\dot{m}{V_c}^2 = \frac{1}{2}\dot{m}w(2V_c + w) \quad (3)$$

It can therefore be determined that the air velocity far below the rotor disk, in the area that is also called the *vena contracta*, is twice the velocity at the rotor

$$v_i \ = \frac{1}{2}w \qquad (4)$$

A relationship between thrust and induced velocity can also be obtained by combining equations 1 and 2:

$$T = \ \dot{m}w = \ \rho A(V_c + v_i)w = \ 2\rho A(V_c + v_i)v_i \qquad (5)$$

$$v_h \ = \sqrt{\frac{T}{2\,\rho A}} = \ (V_c + v_i)v_i = \ V_c v_i + {v_i}^2 \qquad (6)$$

After a few manipulations, the equation becomes:

$$\frac{v_i}{v_h} = -\left(\frac{V_C}{2v_h}\right) + \sqrt{\left(\frac{V_C}{2v_h}\right)^2 + 1} \qquad (7)$$

For the axial climb, it is difficult to determine the area of the *vena contracta*. By simplifying the problem and assuming that the rotor is in a hover, or that $V_c = 0$, we can use the conservation of mass, (1) to derive a relationship between the disk area and the *vena contracta*. As (9) shows, it is expected that there will be a reduction of area of factor 2 far below the rotor disk.

$$\rho A v_i = \rho A_\infty w = \rho A_\infty 2 v_i = 2\rho A_\infty v_i \quad (8)$$

$$\frac{A_\infty}{A} = \frac{1}{2} \quad (9)$$

This reduction in area can be applied to the radius through $A = \pi r^2$:

$$r_2 = \frac{r}{\sqrt{2}} \quad (10)$$

Effective Disk Area

Similarly to aircraft wings, rotor blades suffer losses associated with the formation of vortices at the tip of the blades, also called *induced tip loss.* To quantify these tip losses, Leishman (see ref.) uses what he calls the B factor. This factor is applied to the disk radius, introducing the concept of an effective disk radius and area as shown in (11). The factor B is usually within the 0.95-0.98 range.

$$A_e = \pi (BR)^2 = B^2 \pi R^2 = B^2 A \quad (11)$$

Wake Boundaries in Forward flight

For forward flight conditions, the force vector required is angled forward compared to the hover vector force. This new vector has two components, the rotor lift and the propulsive force. Because of the forward velocity of the rotor, the blades on either side of the rotor disk see a different effective air velocity. This makes the axisymmetric airflow assumption made for hover flight profiles non applicable and hard to predict. However, by looking at experimental data we can get a good idea of what to expect.

Figure 2 shows the location of the rotor blade tip vortices (BTV) for different advance ratios. Advance ratio can be defined as the ratio of the freestream velocity and the propeller tip speed. Although the BTV do not represent the actual boundary of the wake, it can give a good idea of its behavior. Figure 2(a) represents the aft section of the rotor disk while Figure 2(b) represents the forward section of the disk. There is a strong correlation between the position of the overall wake and the airspeed of the aircraft.

For the hover phase, the experimental data from the figure shows that the slipstream diameter narrows as expected. In forward flight, the wake at the front of the rotor disk is displaced towards the center of the disk instead of being pushed in the downward direction. At the rear of the rotor disk, however, the wake is pushed downward as well as displaced further away from the rotor with increasing airspeed.

Airspeed

In the case that no on board ADS is available, the relative airspeed can be calculated from the GPS ground speed and known wind speed. Equation 12 shows this relationship:

$$v_{true} = v_{ground} - v_{wind} \tag{12}$$

Rate of Climb

To determine the rate of climb, the overall vertical distance and the time taken to complete the climb can be used. This method provides a good average rate of climb and is suitable for several situations.

$$ROC = \frac{h}{t} \tag{13}$$

Effects of Altitude

With altitude changes comes changes in atmospheric conditions, namely the temperature, pressure and density of air. The standard atmospheric equations model this phenomenon fairly well:

$$\theta_{std} = (1 - 6.875 \times 10^{-6} ft^{-1}) \tag{14}$$

$$\delta_{std} = {\theta_{std}}^{5.2559} = (1 - 6.875 \times 10^{-6} ft^{-1} \times h_d)^{5.2559} \tag{15}$$

$$\sigma_{std} = {\theta_{std}}^{4.2559} = (1 - 6.875 \times 10^{-6} ft^{-1} \times h_d)^{4.2559} \tag{16}$$

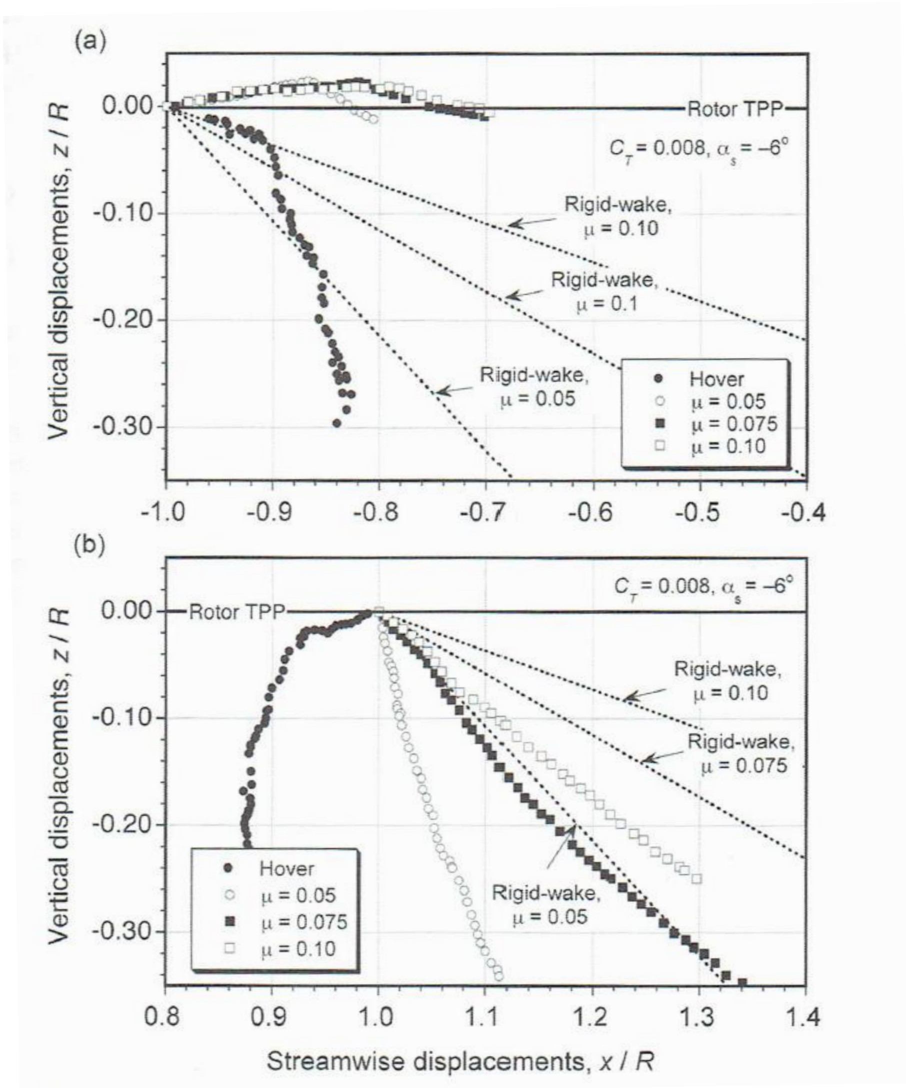

Figure 2 Location of Blade Tip Vortices as a Function of Advance Ratio (μ), Non-Dimensionalized Horizontal Location (x/R), Non-Dimensionalized Vertical Location (z/R).

Figure reproduced with permission from Cambridge University Press. Source: Leishman, J.G. "Wake Boundaries, "*Principles of Helicopter Aerodynamics*, Second Edition, Cambridge University Press, Cambridge, NY, 2006, p. 577

CHAPTER TWO

FLIGHT PLANNING

Methodology

The low operational cost of drones and the accuracy associated with data collected during an actual flight makes the test flight approach an obvious choice. For this reason, flight testing was chosen as the method to complete the objective of this research.

Experimental methods such as *density gradient method,* and *natural condensation effects* are both expensive and difficult to use. Smoke flow visualization is a fairly involved process that requires extensive equipment. Hence, directly measuring the vertical airflow velocity as a function of the radial distance from the octocopter is the most direct and efficient means.

Flight Test Plan

The intended flight profile for NOAA's experiment is to conduct axial climbs to gather data at different altitudes. Because it is expected that the drone will be flying in different atmospheric conditions including wind shear, it was determined that it would be useful to conduct the flight testing at different airspeeds.

Aircraft Description

The subject aircraft is the DJI Spreading Wings S-1000, serial FA39F7RLCK. It is marketed as “designed for high level professional aerial photography and cinematography”. The aircraft’s eight arms and retractable landing gear are made of carbon fiber. Each arm features a 4114 pro electric motor and two high performance 145 mm rotors blades. The motor and blade assemblies form a 15 in (381 mm) diameter rotor. The drone is controlled by the DJI A2 control system, which includes several auto pilot functions. There is also a damped cargo mount. Depending on the outfitted battery, the maximum flight time is about 15 minutes with a max takeoff weight of 11 kg. The empty weight is 4.2 kg. A picture of the drone and key dimensions are shown in Figures 3 and 4.

The auto pilot provides several different control options, such as course lock, home lock, banked turn, etc. The relevant function for this test is the course lock function. This function assists the pilot in having minimal course deviation during the test points. More information about the drone and the A2 controller can be found on the DJI website, www.DJI.com.

Figure 3 Picture of DJI S1000. Source: DJI.com

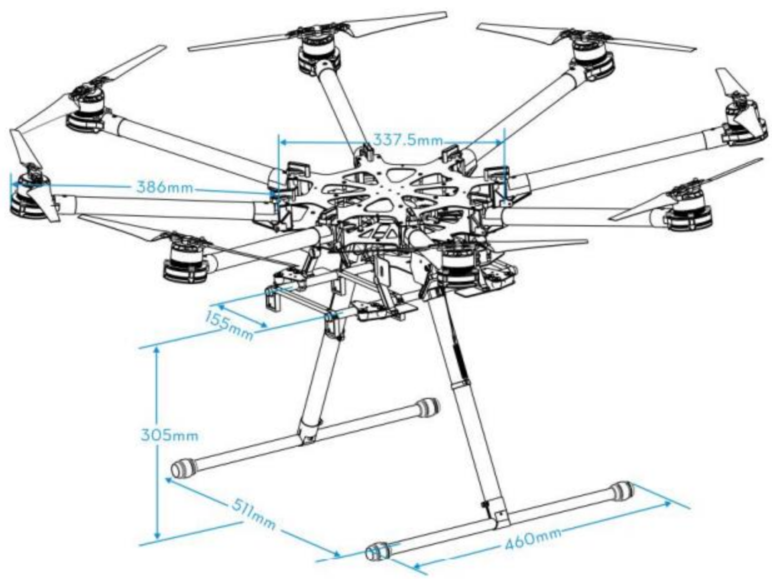

Figure 4 Dimensions of the DJI S1000. Source: DJI

Instrumentation

In order to gather the data, a combination of OEM and custom made equipment were used.

A single aluminum boom was affixed to the cargo mount with the use of a custom made A-frame. Using a combination of rubber collars and standard hardware, three data logging anemometers, model 20250-22 from Digi-Sense, were affixed at different locations on the boom. The distance of the anemometers from the z-datum was -9.45 in (-24.0 cm). The boom assembly weighed 1.13 lbf, (.51 kg) without the anemometers. A measuring tape was affixed to the boom in order to easily measure the positions of the anemometers with reference to the drone y-datum. Details of the testing apparatus can be seen in Figures 5 through 7.

The anemometers weight 1.8 oz (51 g), have a 0.4-20.00 $\frac{m}{s}$ range with a 0.5 Hz sampling rate. They can gather data for several hours. The data can easily be analyzed using the provided software and exported to MS Excel.

Figure 5 Digi-Sense Anemometer.

Figure 6 Boom Assembly

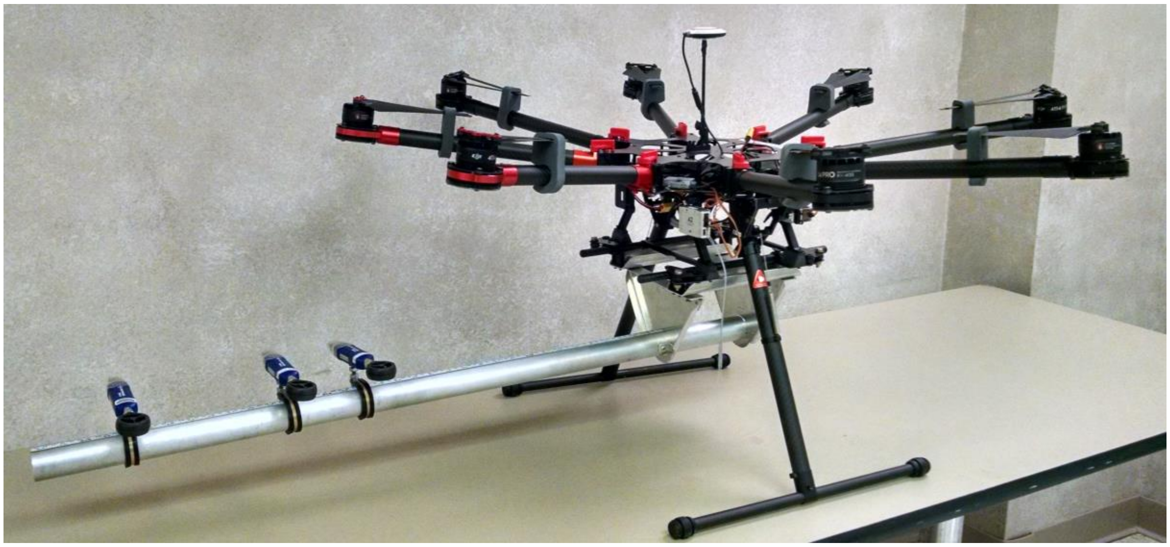

Figure 7 Drone with boom assembly and anemometers

A telemetry system covering several flight parameters was available for the S1000. This however required acquiring proprietary software and equipment from the drone manufacturer. Instead, a simple work around was found and adopted. The iOSD MARK II, which is essentially the drone’s black box, provided the flight data that was essential for the analysis of these test flights. Its sample rate is 200 Hz. More on this can be found in the Data Analysis section of this document.

Data Source and Instruments

Data had to be taken from different sources. A breakdown of the data gathered and their source is given in Table 1.

Table 1 Data Source

	Identifier in device	Corresponding Variable	Unit
iOSD MARK II			
Altitude	GPS Altitude	h	m
Ground speed	Ground Speed	v_{ground}	$\frac{m}{s}$
Heading	Yaw	-	Deg
Time	Sequence	t	Hz
Anemometer			
Time	Date/Time	t	s
Airflow velocity	Value	v_i and V_c	$\frac{m}{s}$
Local wind velocity	Value	v_{wind}	$\frac{m}{s}$
Handheld timer			
Time	-	t	s
Measuring Tape			
Location of anemometer	-	y	in

Test Location

Due to FAA regulations and other basic safety considerations, the areas in which drones can be flown are limited. Also, the flight test technique profile, demanding calm winds to an altitude of 400 ft AGL, required a large open field. Based on these elements, the best suited area to conduct the flight tests was determined to be the Coffee Airfoilers Model R/C Club airfield, at the west end of the Arnold Air Force Base in Tullahoma, adjacent to the base golf club and the Highland Rim Shooters Club. The airfield has a 35 acres treeless area, a 500 ft paved runway, plenty of grassy areas as well as covered working areas perfect for setup and pre and post flight briefings. A GoogleMaps picture can be seen in Figure 8.

Figure 8 Top View of the Airfield. North Directly Up.

Predictions

Based on the theory presented in Chapter One, a few predictions can be made. Knowing that the rotor disk of the drone has a diameter of 0.381 m, we can find the area of the disk and the expected area of the *vena contracta,* A_∞, from (9):

$$A = \pi\left(\frac{d}{2}\right)^2 = \pi\left(\frac{0.381m}{2}\right)^2 = 0.114\ m^2$$

$$A_\infty = \frac{A}{2} = \frac{0.114\ m^2}{2} = 0.057\ m^2$$

$$r_\infty = \sqrt{\frac{A_\infty}{\pi}} = \sqrt{\frac{0.057\ m^2}{\pi}} = 0.13\ m$$

$$\Delta r = r - r_\infty = \frac{0.381m}{2} - 0.13\ m = 0.06\ m = 2.36\ in$$

Since the tips of the rotors reach a distance of 0.71 m from the center of the drone, it is predicted that the boundary of the rotor wake will be at 0.65 m all around the drone:

$$y_{wake} = 0.71m - 0.06\ m = 0.65\ m = 25.6\ in$$

To find the predicted mass airflow and velocities of the flow, the blade tip losses need to be accounted for. Using (11) and assuming a tip loss factor of 0.98:

$$A_e = B^2 A = 0.98^2 \times 0.114\ m^2 = 0.109\ m^2$$

The drone, with all the testing equipment, weighs 6.89 kg (see Appendix for detailed W&B). From this, the required thrust required can be calculated

$$-\vec{F} = T = W = 6.89kg$$

$$v_h = \sqrt{\frac{T}{2\,\rho A}} = \sqrt{\frac{6.89kg}{2\times 1.1\frac{kg}{m^3}\times 0.109m^2}} = 5.36\frac{m}{s}$$

Assuming a constant rate of climb of $V_c = 2.00\,\frac{m}{s}$, the induced airspeed can be determined:

$$v_i = v_h\left(-\left(\frac{V_c}{2v_h}\right) + \sqrt{\left(\frac{V_c}{2v_h}\right)^2 + 1}\right) = 5.36\frac{m}{s}\left(-\left(\frac{2.00\frac{m}{s}}{2\times 5.36\frac{m}{s}}\right) + \sqrt{\left(\frac{2.00\frac{m}{s}}{2\times 5.36\frac{m}{s}}\right)^2 + 1}\right) = 4.45\frac{m}{s}$$

And,

$$w = 2v_i = 2\times 4.45\frac{m}{s} = 8.90\frac{m}{s}$$

We can also make predictions for the conservation of momentum theory for a static hover. Assuming a 1000 ft elevation, the air density can be assumed to be $1.1\,\frac{kg}{m^3}$ on a standard day [Asselin].

$$\dot{m} = \rho A_e(v_i) = 1.1\,\frac{kg}{m^3}\times 0.109\,m^2\times\left(4.45\frac{m}{s}\right) = 0.53\,m^3$$

$$\dot{m} = \rho A_{\infty_e}(w) = 1.1\,\frac{kg}{m^3}\times 0.0545\,m^2\times\left(8.90\frac{m}{s}\right) = 0.53\,m^3$$

The *vena contracta* is usually one and a half to two rotor diameters lower than the rotor disk itself. However, for the research, the anemometers are placed just one rotor diameter below the rotor. It is then expected that the measured values will be somewhere between the theoretical conditions at the disk and the theoretical conditions at the *vena contracta*.

Effects of Altitude

Also, based on (16), the density change for the planned 400 ft climb is less than $5.27 \times 10^{-4} \frac{sl}{ft^3}$. Therefore, this will not be considered as a factor for this research.

CHAPTER THREE

FLIGHT TEST

Flight Test Technique

Axial Climbs

The axial climb flight test technique requires the measurement of vertical air velocity below the drone's rotors, while it ascends at a constant rate of climb. From a static hover starting position and GPS mode set to *on*, the thrust joystick is set and held to a specific position so the drone rises vertically. Once the given altitude is reached, the controls are released and the drone brought back to the ground. The GPS mode is set to *on* to ensure minimal forward and lateral displacement. The maneuver is repeated to measure the vertical air velocity at different locations along the boom.

Since the drone is an axisymmetric aircraft, it can be assumed that the rotor downwash velocities at the rear of the drone when going forward will correspond to the downwash velocities at the front of the drone when going backwards and vice versa. For this reason, the test plan was designed to always have the boom oriented to the front of the drone, while the latter would conduct each test point twice with a 180^{o} heading change. This allows the accurate measurement of airflow velocities both in front and behind the drone with little to no apparatus adjustments.

The following sequence was followed during the axial climb flight test technique:

1. The wind speed was measured on the ground using anemometer and compared to the Tullahoma AWOS III.

2. The anemometers were set up at pre-determined positions on the boom, y_1, y_2, y_3. The position of each anemometer was recorded and CoG calculated using an adapted version of the UTSI Octocopter W & B spreadsheet.

3. The pre-flight was conducted.

4. The handheld timer, anemometers and drone were turned on at the same moment.

5. The run-up and controls check procedures were completed.

6. The drone was set with the boom facing directly into the wind in an out-of-ground-effect hover, and once stable, the pilot began the axial climb holding a constant joystick deflection for 30 seconds, which corresponds to a climb of just under 300 ft. The time was recorded at the beginning and end of all axial climbs.

7. The drone was brought back down and repositioned in an out-of-ground-effect hover and the process repeated for the boom facing away from the wind.

8. Steps 1 to 7 were repeated as necessary. Up to six axial climbs could be repeated with a full battery charge.

Straight Level Flight

The straight level flight technique was designed to mimic moderate wind conditions in which NOAA's apparatus might be required to fly. It measures the vertical air velocity below the drone's rotors, while the drone sees a constant longitudinal airspeed. From an out-of-ground-effect static hover position, the drone is set into a constant altitude and constant speed trajectory for 30 seconds. Once the time is elapsed, the controls are released and without changing the heading, the drone positioned into a static hover position again. The drone is set into a reverse constant altitude and constant speed trajectory for 30 seconds. The maneuver is repeated for different airspeed and anemometer locations. The same axisymmetric assumption as for the axial climb flight test technique is made here.

The following sequence was followed during the straight level flight test technique:

1. The anemometers were set up at pre-determined positions on the boom, y_1, y_2, y_3. The position of each anemometer was recorded and CoG calculated using an adapted version of the UTSI Octocopter W & B spreadsheet.

2. The power settings to be tested were pre-programmed in the remote control.

3. The pre-flight was conducted.

4. The handheld timer, anemometers and drone were turned on at the same moment.

5. The run-up and controls check procedures were completed.

6. The drone was set with the boom facing directly into the wind in an out-of-ground-effect hover. Using the pre-programmed power setting, the pilot put the drone in constant forward airspeed and altitude motion for 30 seconds. The time was recorded at the beginning and end of the maneuver.

7. The drone was brought to a stop without changing altitude or heading. Using the same pre-programmed power setting, the pilot put

the drone in constant velocity and altitude motion for 30 seconds in reverse. The time was recorded at the beginning and end of the maneuver.

8. Steps 6 and 7 were repeated with different power settings. Up to six straight level flights could be completed with one battery charge.

Test Conditions

Initial flight tests were conducted early in the morning, at about 8AM. It was quickly realized that the air mass near the ground was not stable enough to gather quality data. Flight testing was moved to 6AM, which was one hour after sunrise for this time of the year. Test days with wind forecast higher than $3\,\frac{km}{h}$ were rescheduled. The combination of mechanical and weather related delays caused the testing to be spanned over a period or six weeks. In total, there were nine flight test days.

The team was composed of two members; a pilot and a lead test engineer. The pilot was a contractor with drone flying experience. The test engineer was the author of this research paper.

The pilot and test engineer were positioned at a lateral range of 50-150 ft from the drone at all times to ensure that a good perspective could be achieved, without compromising the quality of the visual cues.

For all flights, the CoG was kept in the ranges given in Table 2. Note that the CoG in x and z were constant throughout all tests. Figure 9 gives a schematic of the axes orientation on the drone. A print out of the spreadsheet used to calculate the CoG is shown in the appendix.

Table 2 CoG Range During Test Flights

Axis	Position Range in (mm)
x	0.02 (0.5)
y	2.15 to 2.56 (56 to 65)
z	-2.25 (-57)

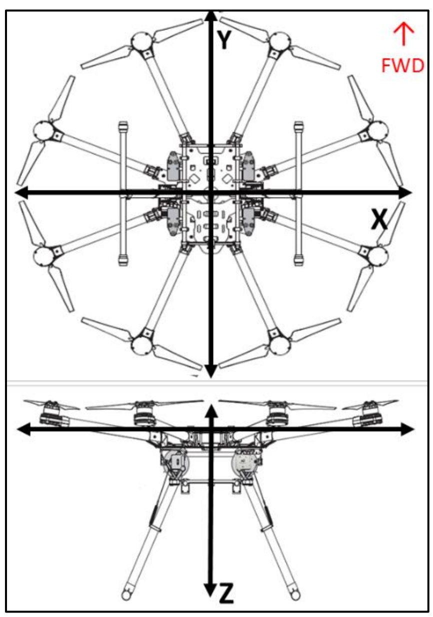

Figure 9 Representation of Drone Axes

During the axial climbs, it was noted that it took about 10 seconds for the drone to stabilize into its new attitude. When looking at the data, this time band seemed to be consistent throughout most test points and thus it was decided to remove it from the data analysis.

After the 10 second stabilization period, the drone sometimes oscillated for short period of time. It is suspected this was the autopilot responding to either a wind gust or possibly the extra drag generated by the boom. The amplitude of these oscillations was about 6 in (15 cm) at the end of the boom. The biggest oscillations observed had an amplitude of 2 ft (0.6 m) at the end of the boom. The drone was immediately brought down to the ground and battery voltage found to be low. It was determined that the low voltage of the battery had triggered the power saving mode which limits the power inputs to the motors. The tests were ended for the day.

Flight Planning

The lack of telemetry made it difficult to ensure that set test parameters were respected during the test point. For example, altitude, velocity, heading, ROC and GPS track had to be judged by eye. Below is a description of how these limitations were mitigated.

Rate of Climb

The best way to regulate this parameter was to complete axial climbs at different rates and correlating them to joystick positions. The controls position for a ROC of 2.5 m/s was determined and used for all axial climb test points.

Velocity

Equation (12) provides a viable way to calculate true airspeed from local winds and GPS ground speed. However, due to the possibility of the local wind conditions changing, this method was not used. Instead, similar to the ROC method covered in the previous paragraph, straight horizontal flights were completed at different power settings and correlated to the GPS ground speed data from the MARK II. The remote controller had the capability to hold three pre-programed power settings. This feature was helpful in that using the A2 controller to manage the power setting allowed to hold a power setting accurately, and by extension kept the airspeed constant. This was a more accurate method than having the pilot roughly guess joystick position inputs. The determined correlation between power setting and airspeed is shown in Table 3:

Table 3 Correlation Between Power Setting and Longitudinal Airspeed

Power Setting (%)	Airspeed (m/s)
30	3
40	4
50	5
60	6
70	7
80	8
90	9
100	10

Altitude

This parameter had to be measured roughly by sight. When at low altitudes, the main criteria was to stay out-of-ground-effect. To achieve this, the points were conducted at a conservative distance from the ground. The maximum FAA permitted altitude for drones of this type is 400 ft. In order to respect this limit, the duration of each climb was limited to 30 seconds at a ROC of 2.5 m/s, which gave a healthy 150 ft (45m) safety margin. When excluding the settling down time of 10 seconds, each test point had about 10 usable data points.

Axial Stability

Conducting axial climbs without any lateral and longitudinal displacements was key to this research. Fortunately, the autopilot features a GPS location lock mode. This allowed the drone to stay within a *rising cylinder* of 1.5 m radius. To ensure the location lock mode was functioning properly, the MARK II GPS data was plotted and the straight climbs were confirmed to stay within the expected

1.5 m radius cylinder. The down side to this flight mode is that the auto pilot can make sharp corrections to the drone's attitude and induce scatter in the data.

Heading

This parameter was also a very important characteristic of the test since the drone had to be directly facing the wind or away from it. It was found to be accurate and practical to align the data boom with the windsock of the airfield. This allowed for timely adjustments in the case of wind direction shifts between test points.

Battery Life

The only voltage-remaining indication on the drone is an LED light that changes color when low voltage levels are reached. According to the manufacturer, the S1000 has an expected flight time of about 15 min. A few trials conducted at the beginning of the research found that the flight time was closer to 7-10 minutes, depending on the power requirements of the maneuvers flown. Flight planning was very important to ensure that as many test points as possible could be conducted for each battery charge. The drone was also set down at strategic moments to measure the battery voltage and ensure enough power was left to continue safely. Full battery charging takes about 1 hour, which pushed the test times too late in the morning to continue flight testing with suitable atmospheric conditions.

Data Recording

Although there was no live telemetry from the drone, all data was recorded either on the MARK II or the internal memory of the anemometers. The MARK II is hard mounted in the drone and can essentially be used as an FDR: it contains all flight parameters of the drone. The anemometers contained only readings of the air velocity. It is to be noted that MARK II file sizes needed to be kept under 100 MB. Care was taken to not have the drone under power for more than 15 consecutive minutes to keep the file sizes below that threshold.

Data Extraction and Analysis

Data Extraction

As discussed in the apparatus section of Chapter One, flight data from the drone itself was not available in real time. All flight data was required to be downloaded after each flight. This section covers the procedure used to access the data required from the drone and test apparatus. Also, a description of all the software used is available in Table 4.

The download procedure for the anemometers data was fairly simple. Through the Digi-Sense proprietary software named *Anemometer DL*, the data was downloaded to a computer and exported to Excel using the export function. With minimal data formatting, the data was ready for plotting.

The MARK II creates a DAT file every time power is applied to the drone and records several flight characteristics at a sample rate of 200 Hz. DAT files were downloaded through a micro-USB cable from the MARK II to a computer using the DJI WIN Driver and DJI iOSD Assistant software. The DJI Data Viewer software available on the manufacturer's website to analyze the data has extremely inadequate functions. One of its biggest limitations is that it does not allow the export of data. A third party website, www.mapsmadeeasy.com, was used to convert the DAT files into CSV files. Microsoft Excel was then used for the analysis and formatting of the CSV files.

Table 4 List of Software

Software Used	Type	Version	Source	Use
DJI iOSD Assistant	Application	4.1	DJI.com	Download data from MARK II
DJI Data Viewer	Driver	N/A	DJI.com	Download data from MARK II
Anemometer Data Logger	Application	2.3	Provided with instruments	Set and download data from anemometers
Log_viewer	Website	N/A	www.mapsmadeeasy.com	DAT to CSV conversion

Rate of Climb

No ROC was included in the exported CVS files. This parameter had to be calculated using (13), from the GPS altitude and time recorded by the MARK II.

Based on the GPS altitude accuracy of ±1 m, using this method gave a rate of climb with a small error. For a 30 second 75 m climb, which is the typical axial climb flown for this research, this corresponds to an error of about a $0.1 \frac{m}{s}$ difference or 3%.

True Airspeed

For the straight level flights, true airspeed was required but since the drone does not have an ADS, an alternate method was used. The airspeeds were determined using Table 3 and the specific power settings used for the test point.

Vertical Airflow Velocity

The sourced anemometers did not provide a means to determine positive from negative airflow velocity values. In most cases, this did not prove to be a problem since the flow direction could be determined based on the flight profile. However, it complicated the data analysis for time periods when the drone was oscillating. The sensitivity of the instruments allowed the hectic flow conditions to be documented. Instead of showing airflow moving in both directions due to the vertical oscillations, the data showed trends of changing positive velocities. Also the length of the boom caused the effects of the oscillations to be non-negligible. Care had to be taken to not confuse these for actual airflow increases around the drone. Figure 10 shows the anemometer data plotted for an axial climb test flight.

On the left are the results for readings at positions 20, 23 and 29 in (51, 58 and 74 cm) top to bottom, and on the right are results for 21.5, 25 and 32 in (55, 64 and 81 cm). The highlighted sections are test points.

Heading

To confirm that there were no errors made with the drone orientation with respect to wind, the field from the MARK II named *yaw* was observed during data analysis. This field gives data readings between -180º and 180º, with 0º to -180º degrees corresponding to 180º to 360º and 0º to 180º corresponding to 0º to 180º. The accuracy of this parameter was not known so it was not used for any other purpose.

Stabilization Period

As mentioned earlier, data analysis required often to ignore points related to the transition periods. Figure 11 shows examples of test points with and without transition periods. For stable test points, the data clearly showed the end of the transition period, and it usually did not last longer than 10 seconds.

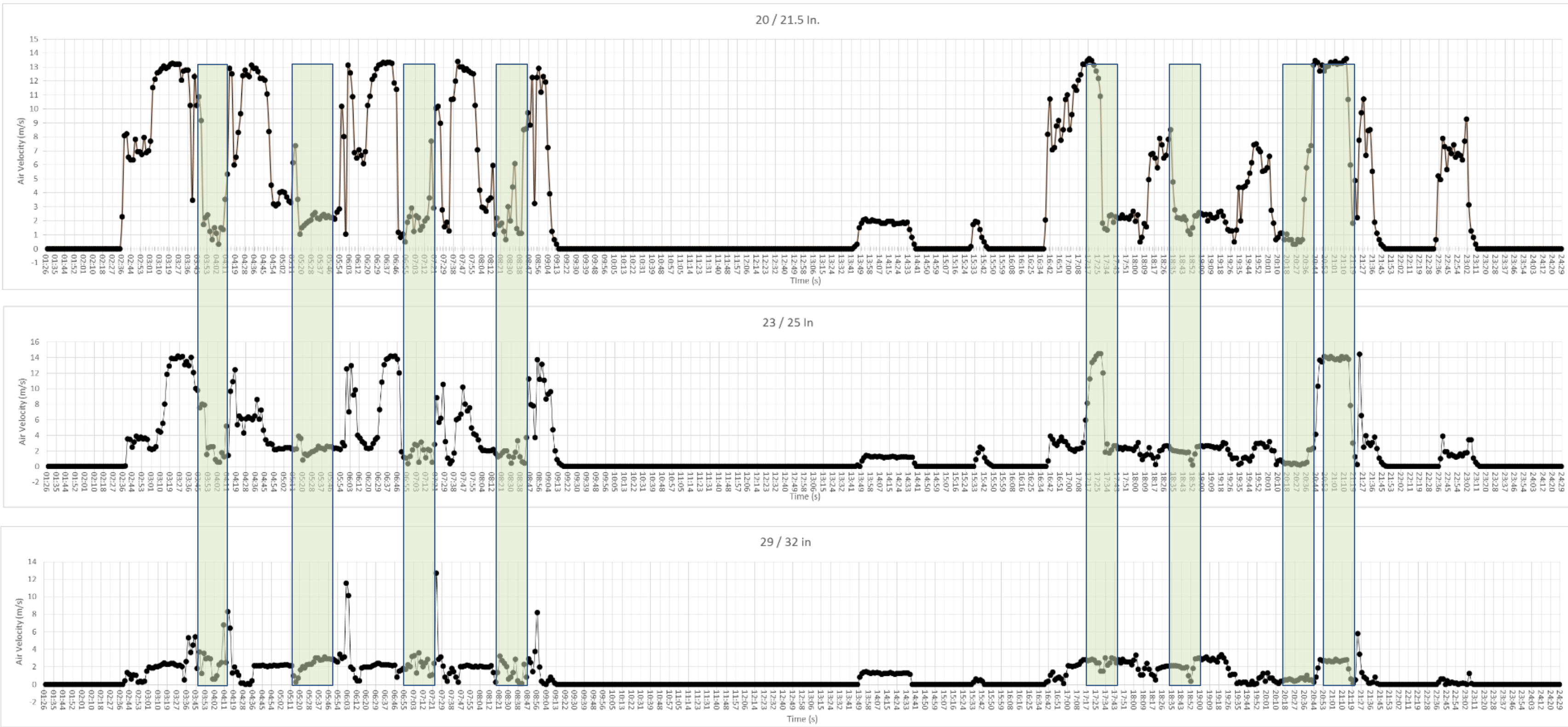

Figure 10 Example of Anemometer Data Plot

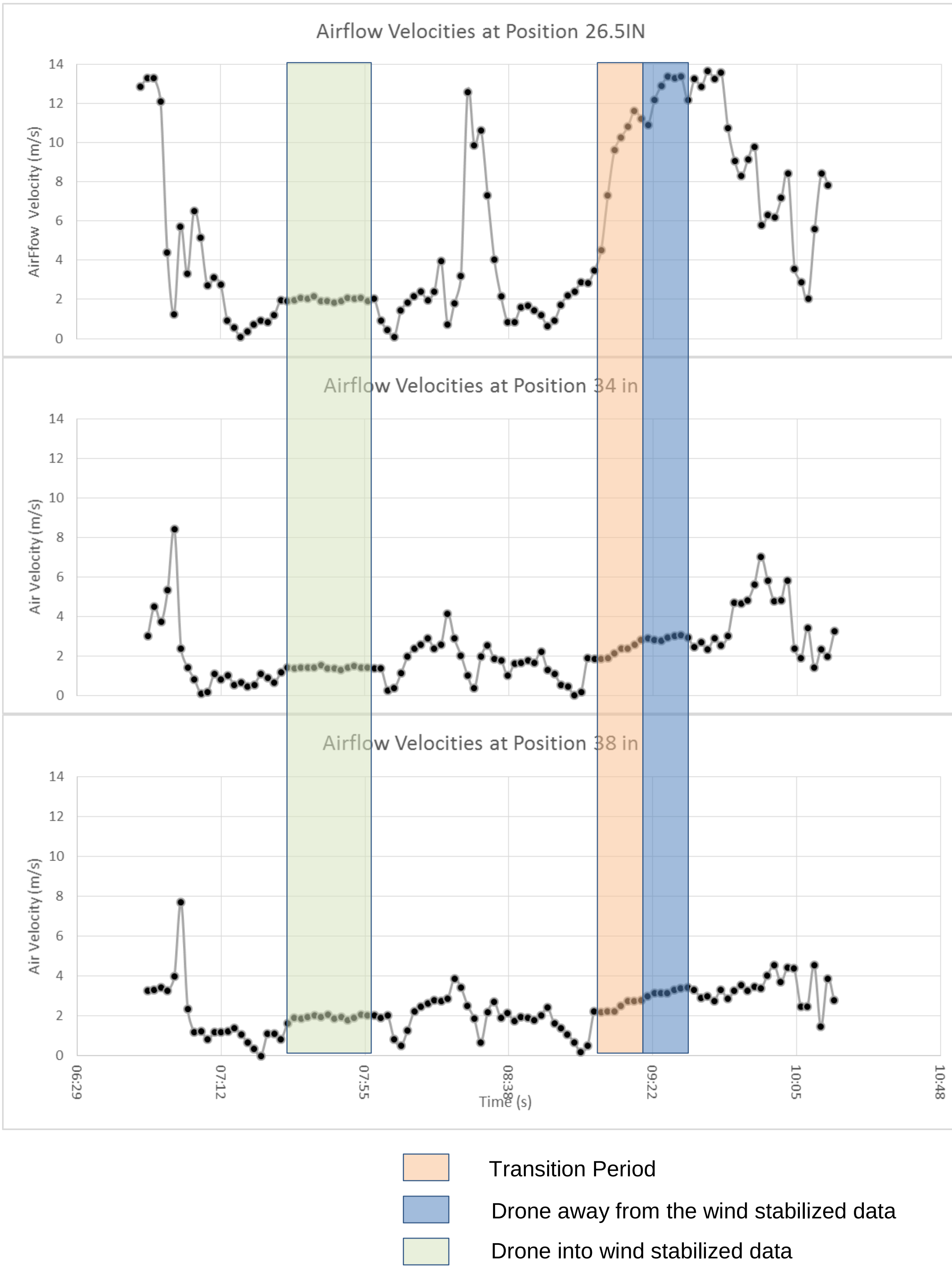

Figure 11 Anemometer Data Plot with Example of Data Editing

CHAPTER FOUR
RESULTS AND DISCUSSION

Axial Climb Results

For the axial climbs, the resulting downwash velocity profiles and associated one standard deviation errors are plotted in Figure 12. Even in calm winds, less than $3\frac{km}{h}$, significant differences were found between the drone facing into the wind and facing away from the wind.

First, the stability of the drone seemed to be compromised when the boom was downwind. On Figure 12, this is seen in both the size of the standard deviation errors and in the increase of data scatter in the 30 to 38 inch (76.2 to 96.5 cm) range. They are both a result of the small oscillations of the drone in pitch and roll which caused the anemometers to measure strong velocity gradients. Despite this data scatter, the plot clearly shows the rotor downwash limits.

Second, when facing into the wind, the rotor downwash ended at 24 in (61.0 cm), versus 27.5 inches (69.8 cm) when the drone was facing away from the wind. The forward limit of the downwash is within 5% of the 25.6 in (65.0 cm) theoretical value. However, the 3.5 in (8.9 cm) difference between the front and rear limits is bigger than what was expected and is considered a significant difference for winds lower than $3\ \frac{km}{h}$.

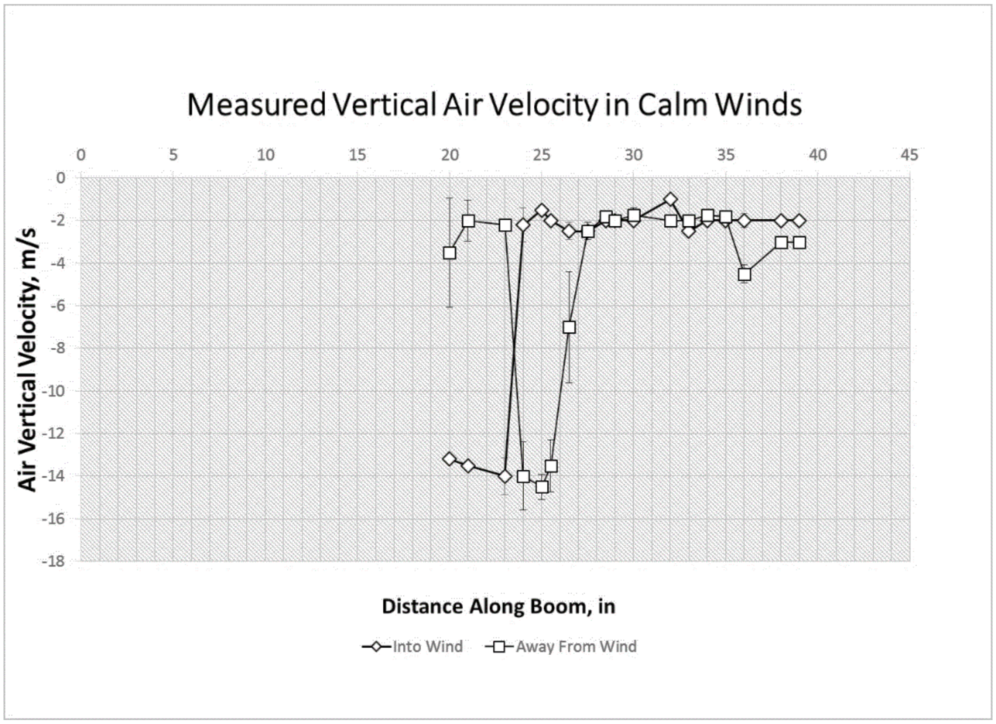

Figure 12 Airflow Velocities for Axial Climb

Third, an interesting phenomenon is shown in the *away from wind* data of Figure 12. The slipstream is only present between 23 in (58.4 cm) and 27.5 in (69.8 cm). Outside of this range, there was no downward velocities corresponding to downwash. This shows the size of a single rotor slipstream is 4.5 in (11.4 cm). This is smaller than the predicted 5.1 In (13.0 cm).

After subtracting the ROC, V_c, from the airflow velocities, Figure 13 was obtained. This illustrates the induced airflow velocities, v_i, around the drone. Of note is that the velocities are not exactly zero. This was a surprising result because of the small standard deviation obtained through the anemometer data, and the small error presented by the ROC calculations ($0.1\,\frac{m}{s}$). It is suggested that the reason for this difference is the calibration of the anemometers. However, since the data recorded showed consistence throughout the flight tests, it is not believed to have a negative impact on the resulting conclusions of this research.

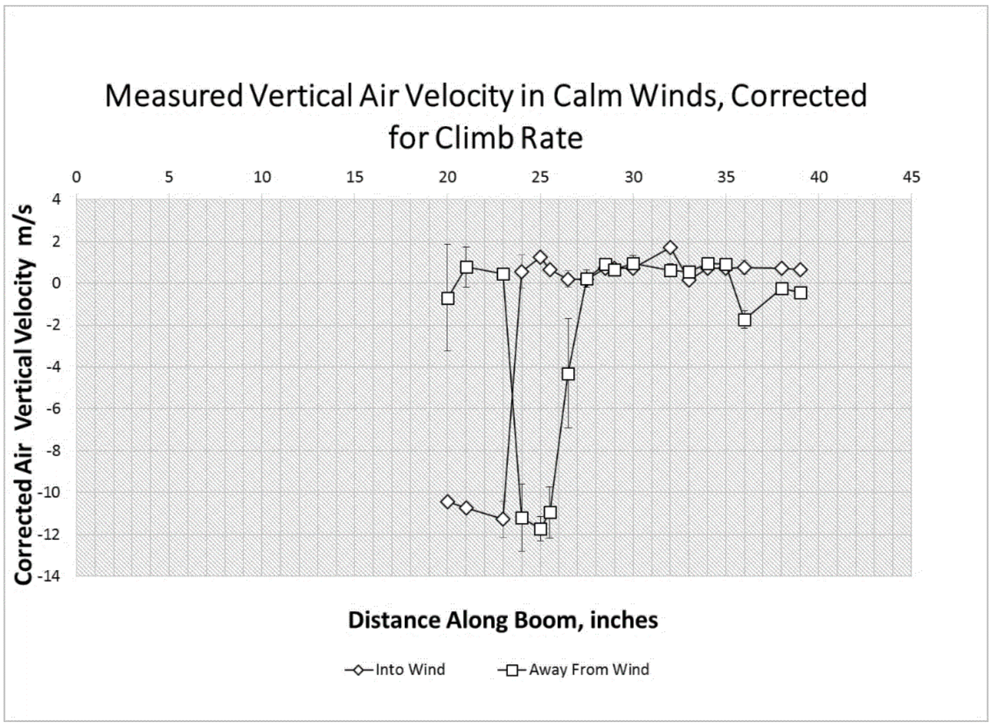

Figure 13 Airflow Velocities for Axial Climb, Corrected for Climb Rate

Straight Level Flight Results

For the straight level flights, the resulting downwash velocity profiles are plotted in Figure 14 for $3\,\frac{m}{s}$ and Figure 15 for $4\frac{m}{s}$. It is clear for both cases that the slipstream at the front of the drone moves towards the center of the drone, further than 22 in (55.9 cm). Because of the increased instability of the drone at higher

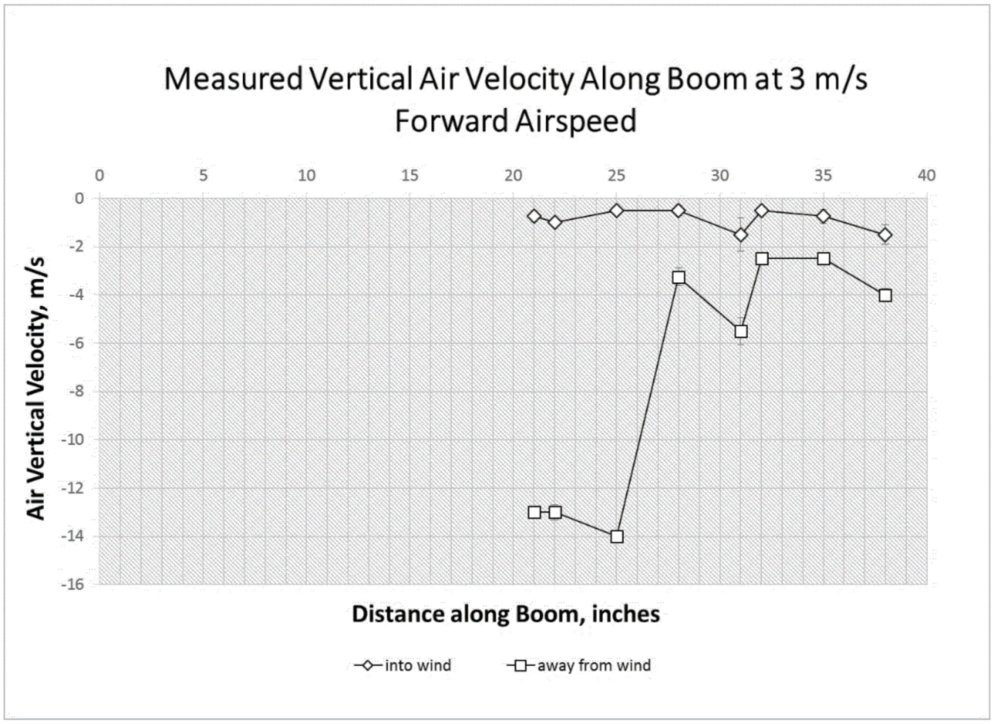

Figure 14 Airflow Velocities for 3 m/s Airspeed

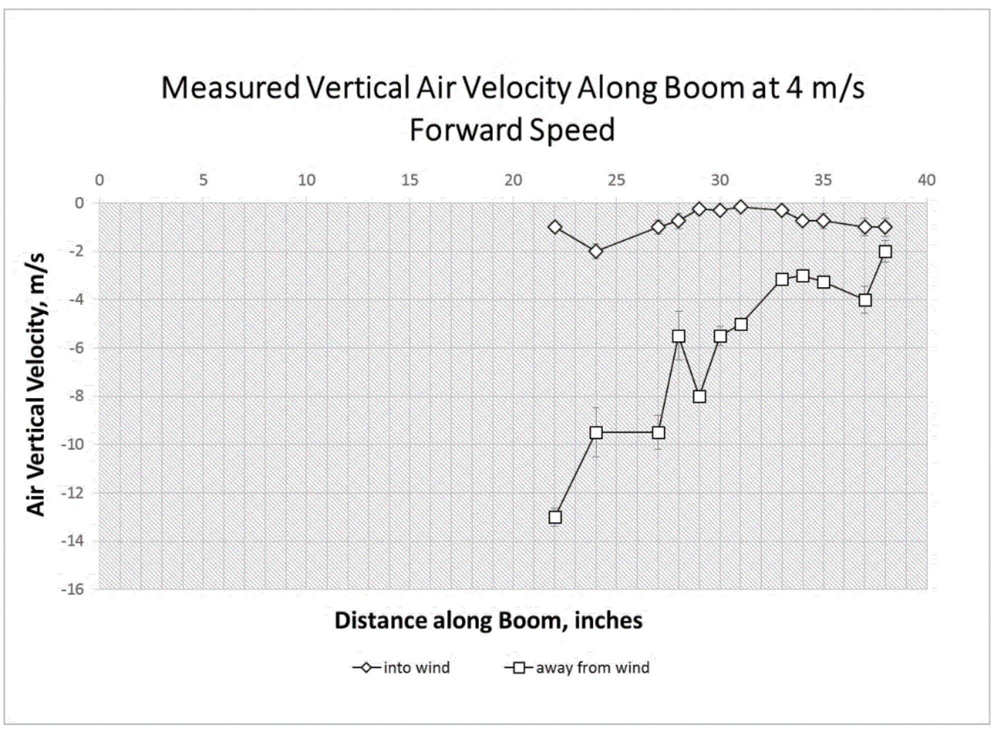

Figure 15 Airflow Velocities for 4 m/s Airspeed

speeds, the exact limit of the slipstream at the back of the drone requires more analysis.

An educated guess can be made, however, by assuming that all data points showing a velocity equal or lower than the forward airspeed is part of the forward velocity component and not the rotor downwash. For the $3\frac{m}{s}$ case, this means that the slipstream ends at 32 in (81 cm). For the $4\frac{m}{s}$ case, the slipstream ends at 33 in (83 cm). This confirms the theoretical trend of the slipstream to be displaced further to the rear as velocity increases.

Another point worth noting is the increasing level of scatter in the data as the airspeed increases. Typical data from airspeeds of $2\frac{m}{s}$, $3\frac{m}{s}$ and $4\frac{m}{s}$ are shown in Figure 16. The standard deviations for the data gathered at $2\frac{m}{s}$ and $4\frac{m}{s}$ airspeeds at the 28 in location are 0.12 and 1.54 respectively. The difference between these two standard deviations is significant and is thought to be caused by the decrease in the drone's stability as its airspeed increases.

Summary of Results

To help visualizing the rotor downwash profile around the drone and the differences between wind speeds, Figure 17, 18 and 19 were created. Since the drone is axisymmetric, the data captured for the away from the wind phase was used to represent the downwash profile behind the drone in forward flight. The figures clearly show the displacement of the rotor slipstream towards the rear.

Also, Figure 17 shows well that airflow patterns corresponding to a rotor slipstream is only present between the -23 in (-58.4 cm) and -27.5 in (-69.9 cm) positions. The predictions made earlier were an individual slipstream of about 10.2 in (26.0 cm), which is more than twice as big as the measured number, 4.5 in (11.4 cm).

Figures 20, 21 and 22 present a top view of the slipstream limits caused by the rotor downwash for the different wind speeds tested. The displacement of the slipstream towards to rear can be clearly seen, with the phenomenon amplifying with wind speed increases. The predicted limits for calm winds is also shown for comparison purposes.

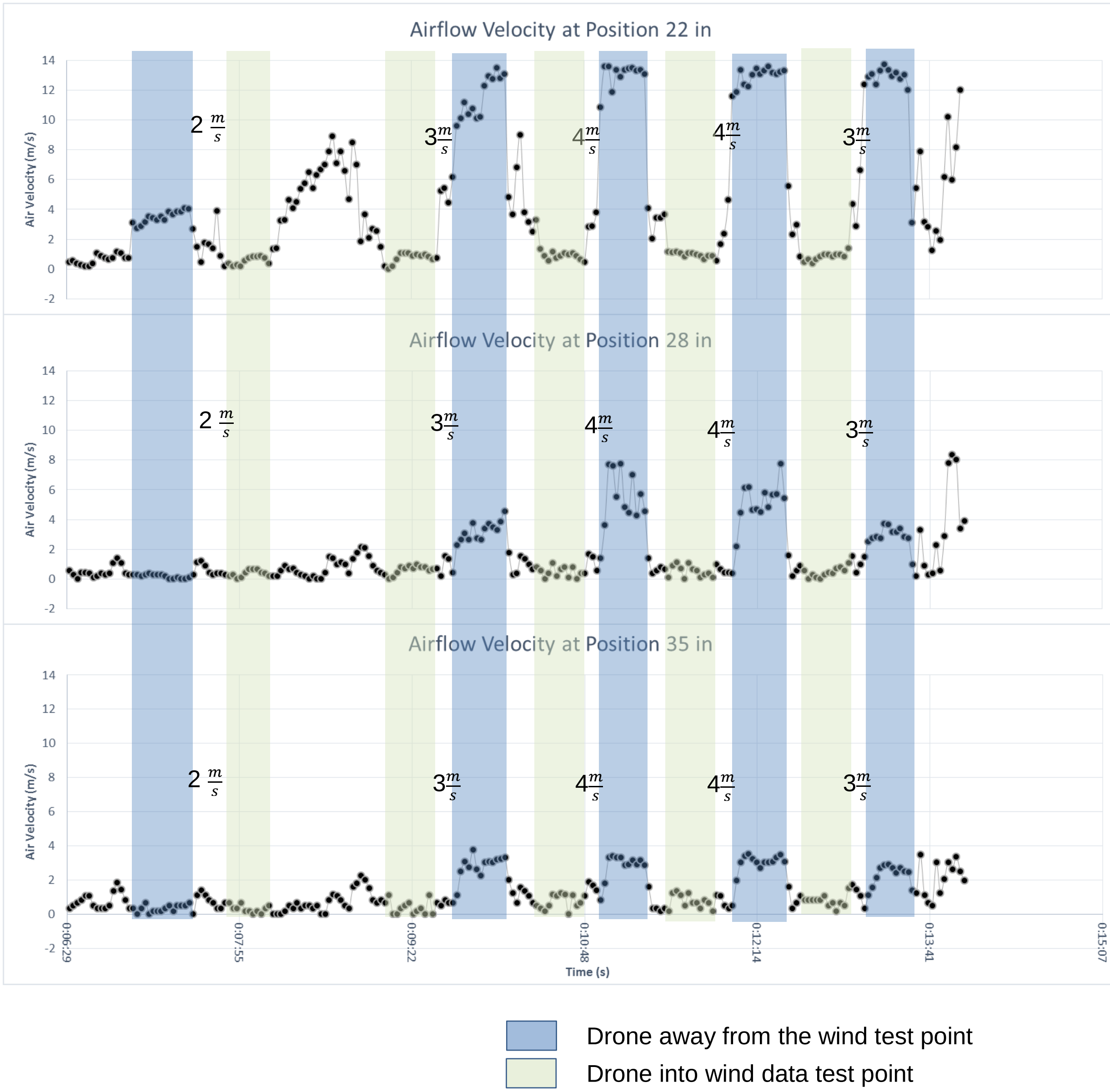

Figure 16 Airflow Velocities for Straight Level Flights at 2m/s, 3 m/s and 4m/s Airspeeds

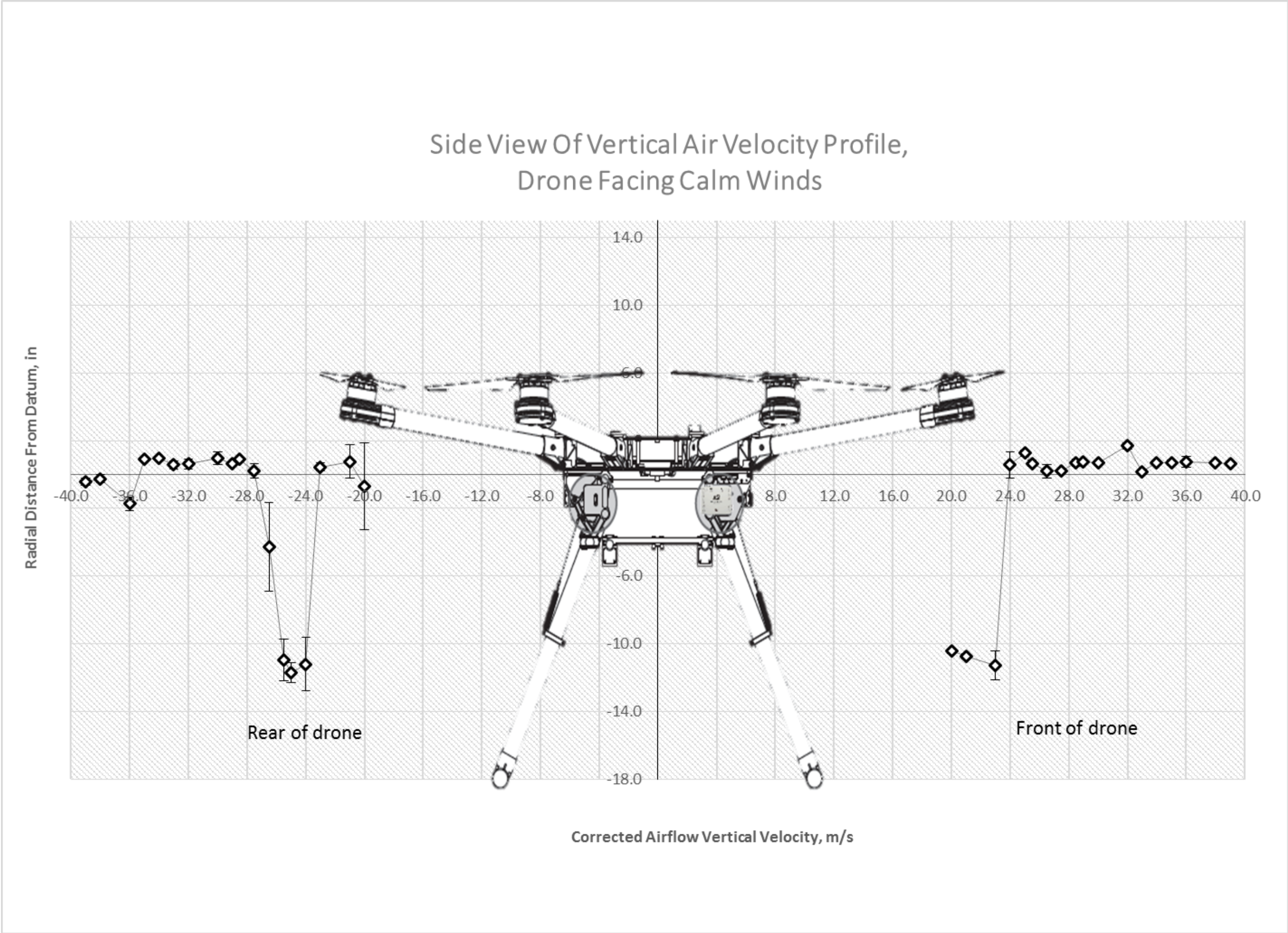

Figure 17 Airflow Profile Around Drone During Axial Climb

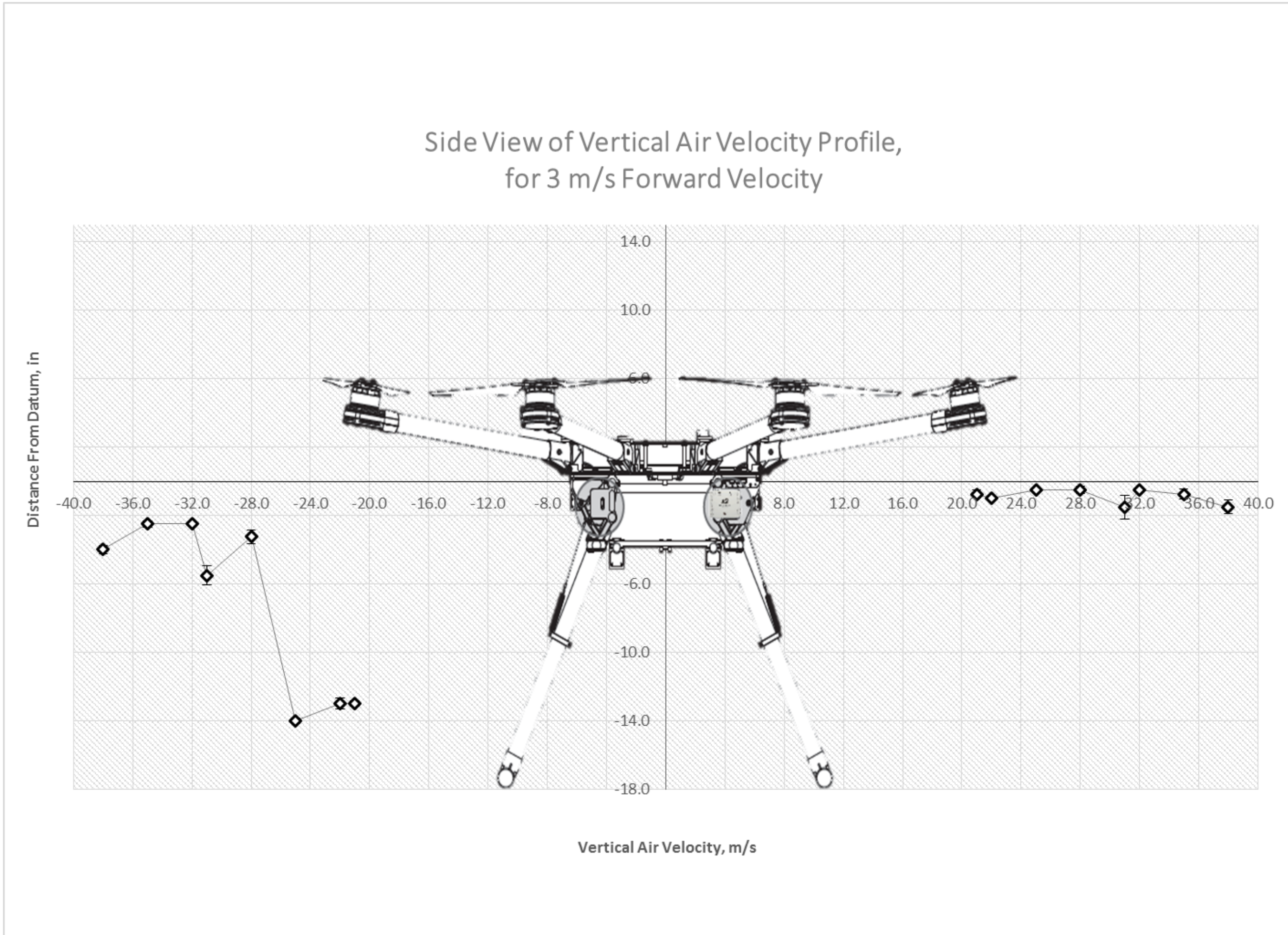

Figure 18 Airflow Profile Around Drone with 3 m/s Airspeed

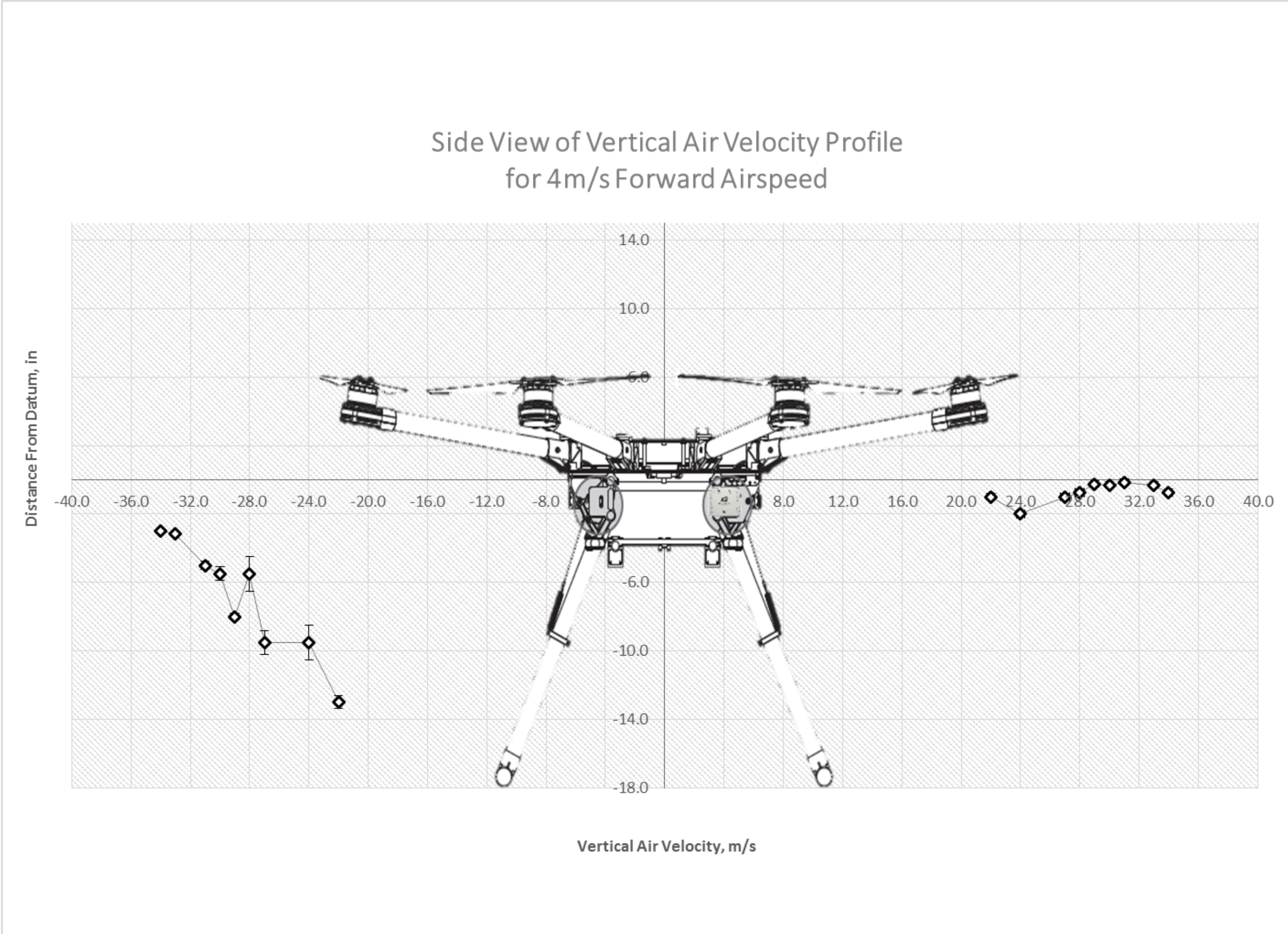

Figure 19 Airflow Profile Around Drone with 4 m/s Airspeed

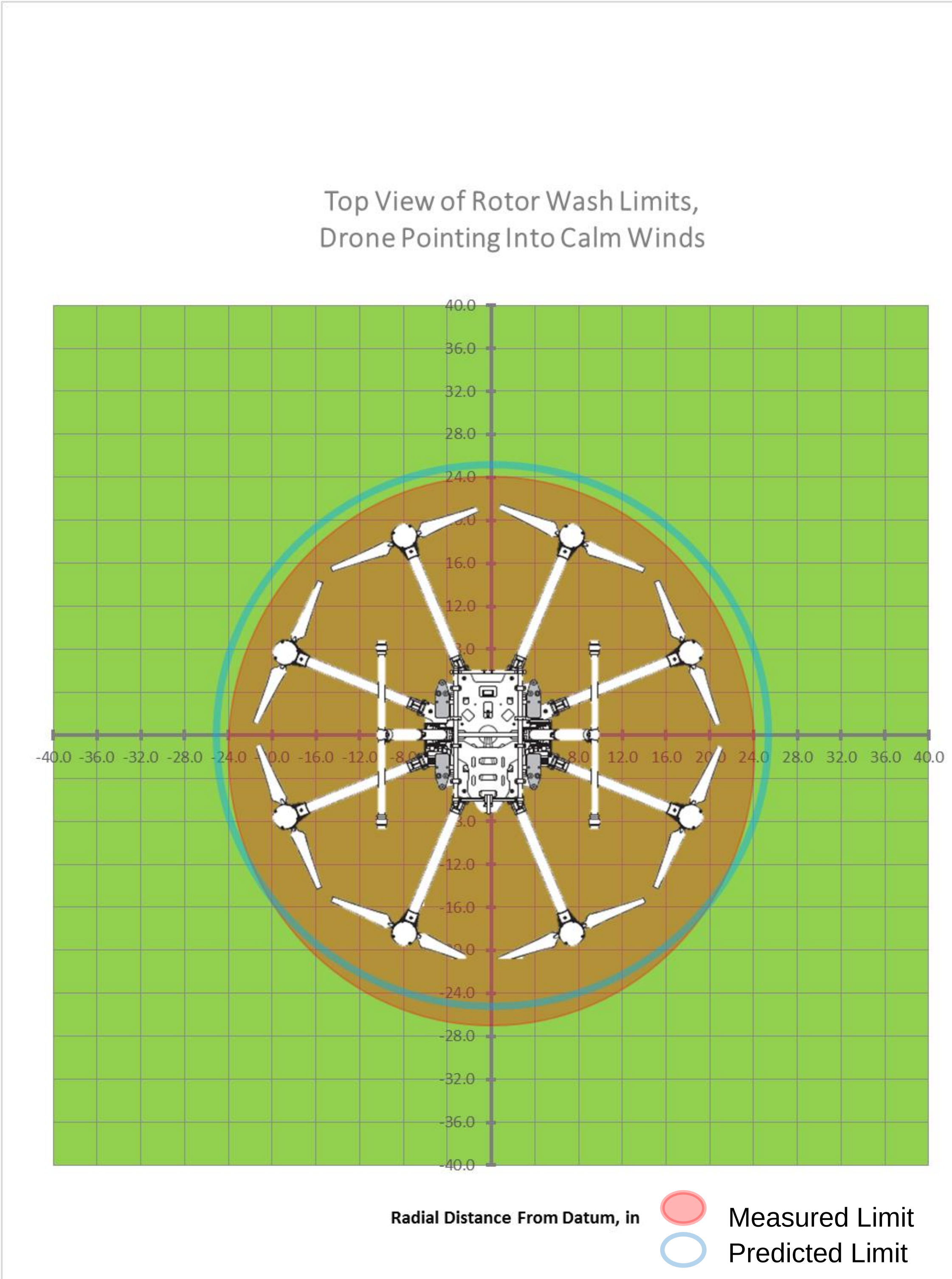

Figure 20 Top View of Drone Slipstream in Axial Climb

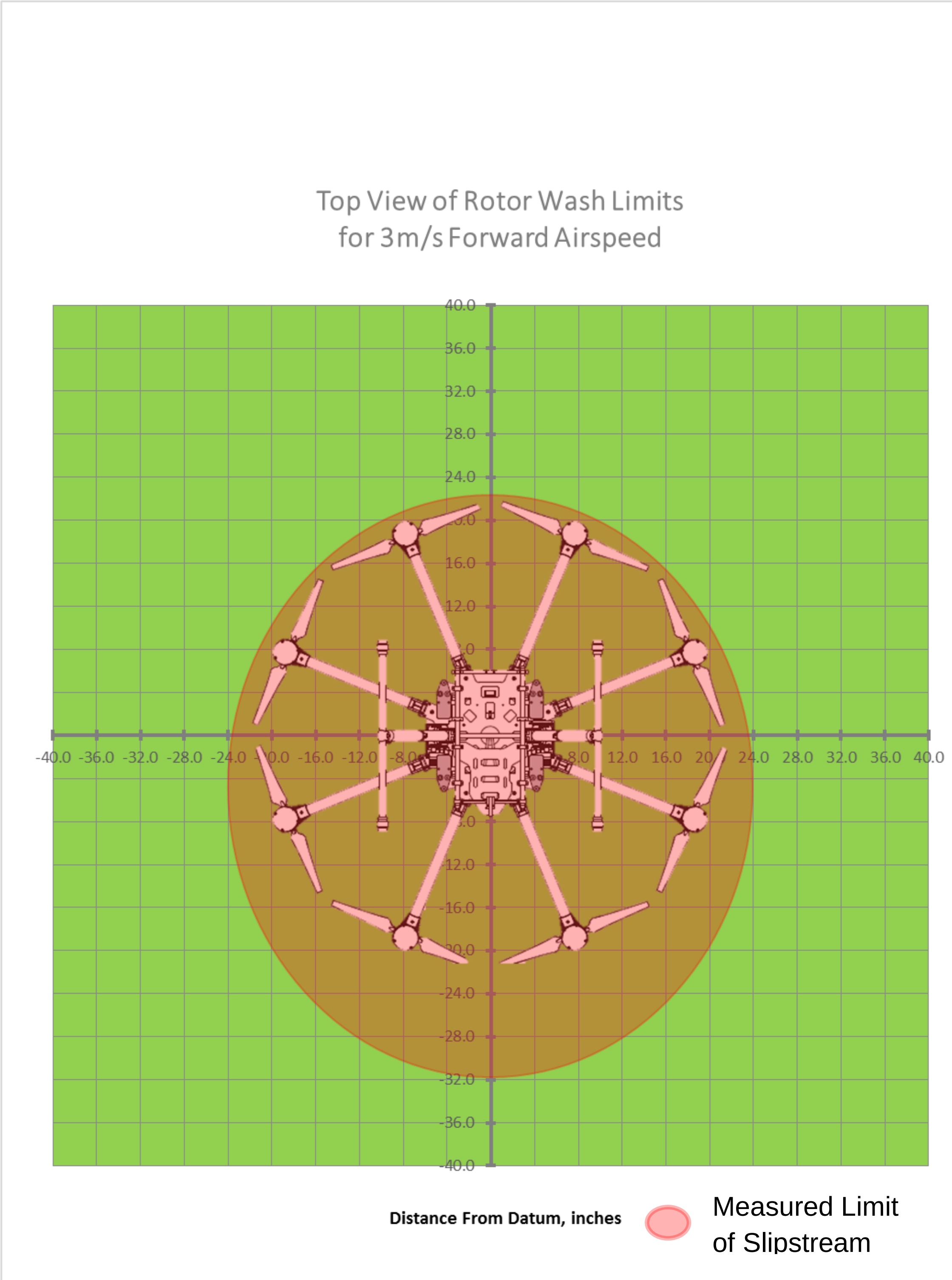

Figure 21 Top View of Drone Slipstream in 3 m/s Airspeed

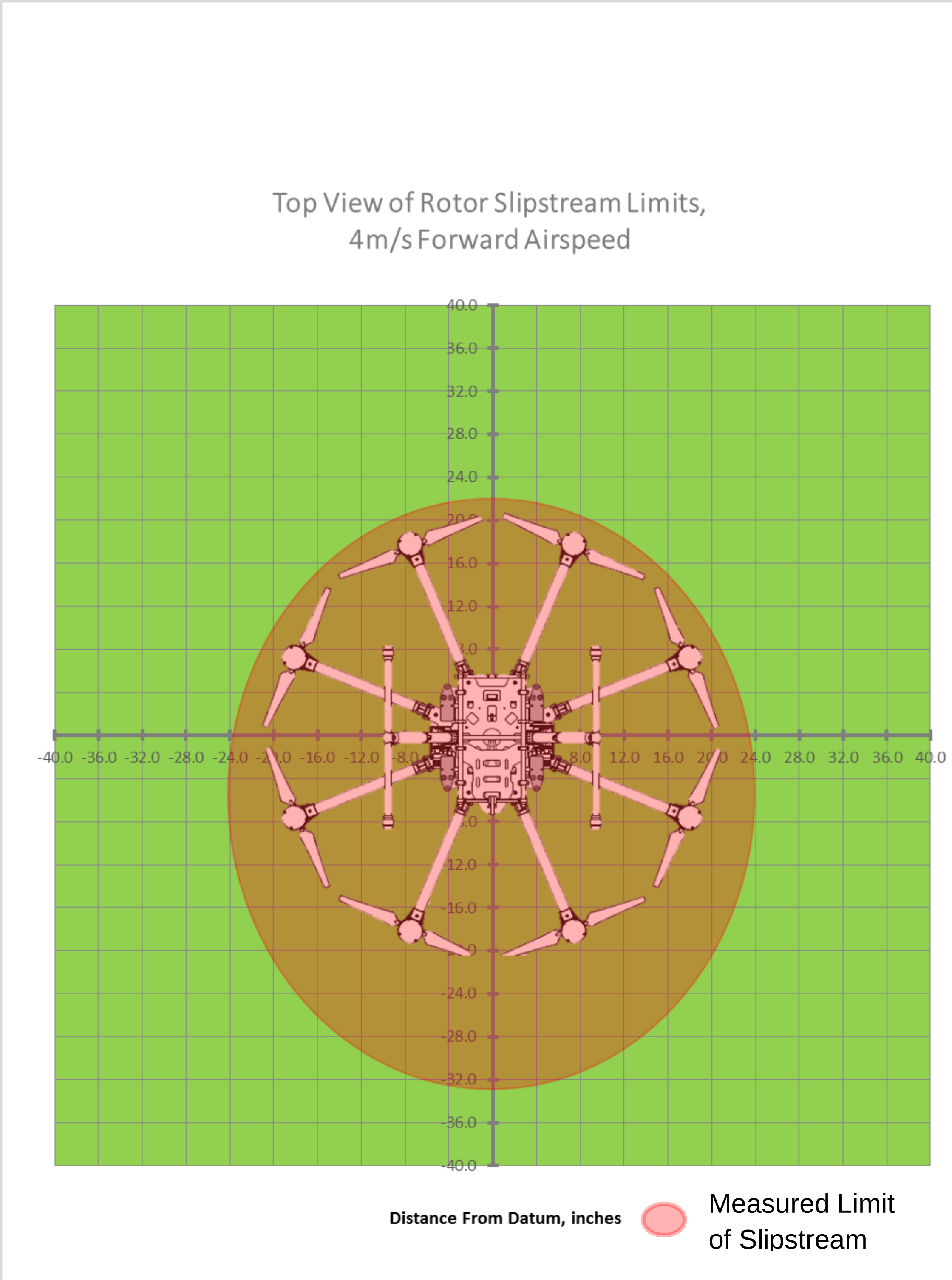

Figure 22 Top View of Drone Slipstream in 4 m/s Airspeed

CHAPTER FIVE
CONCLUSIONS AND RECOMMENDATIONS

Conclusion

The purpose of this research was to determine the slipstream limits of the rotor downwash on the DJI S1000 Spreading Wings octocopter. Anemometers attached to a custom made boom were installed on the drone cargo frame and two flight test techniques were performed: axial climbs and straight level flights. The axial climb provided good and stable measurements while gathering meaningful data for the straight level flights proved to be more challenging. It was determined that axial climbs in calm wind conditions displaced the rotor downwash slipstream up to 3.5 in (9 cm) towards the rear of the drone. The 24 in (61 cm) limit of the slipstream at the front of the drone was within 5% of the theoretical model. The measured size of individual rotor slipstreams and slipstream positions were half the size of the theoretical values. For the $3\,\frac{m}{s}$ and $4\,\frac{m}{s}$ cases, the slipstream limit at the front of the drone moved closer than 22 in (56 cm) while the limit at the rear of the drone moved to 32 in (81 cm) and 33 in (84 cm) respectively.

Recommendations

The following recommendations are made to NOAA for their use of the S-1000 a part of their drone program:

1. Instruments should be installed at least 30 in (76.2 cm) from datum. This will give a 6 in (15.2 cm) buffer between the slipstream limit and the instrument.

2. Avoid gusty and windy atmospheric conditions. Conducting measurements in constant winds lower than $3\,\frac{m}{s}$, or $5\ kts$, will ensure minimal drone oscillations and best data quality.

3. Axial climbs should always be conducted with the boom facing into the wind.

4. Ensure the drone is well stabilized in a static hover before beginning each axial climbs. This will help minimize the stabilization period of the drone while climbing.

LIST OF REFERENCES

1. Leishman, J.G. “Fundamentals of Rotor Aerodynamics,” *Principles of Helicopter Aerodynamics*, Second Edition, Cambridge University Press, Cambridge, NY, 2006, pp. 55-101.

2. Leishman, J.G. “Wake Boundaries,” *Principles of Helicopter Aerodynamics*, Second Edition, Cambridge University Press, Cambridge, NY, 2006, pp. 577.

3. Kimberlin, R. D. *Flight Testing of Fixed-Wing Aircraft*, AIAA, Reston VA, 2003.

4. Asselin, M. “Appendix B: Atmosphere,” *An Introduction to Aircraft Performance*, AIAA, Reston, VA, 1997, pp. 309-315.

5. Solies, P. *Fixed Wing Performance Flight Testing* [PowerPoint slides] University of Tennessee Space Institute, Tullahoma, Tn, 2015.

6. DJI Innovations, *Spreading Wings S1000 User Manual*, V1.10, Shenzhen, China, 2014.

7. DJI Innovations, *A2 User Manual,* V1.24, Shenzhen, China, 2016.

8. DJI Innovations, *iOSD MARK II User Manual*, V2.2, Shenzhen, China, 2016.

9. DJI Innovations, *DJI S-1000 Specifications Sheet* [webpage] DJI.com/products/S1000 [retrieved 12 May 2016].

10. DJI Innovations, *DJI A2 Specifications Sheet* [webpage] DJI.com/products/a2 [retrieved 12 May 2016].

11. DJI Innovations, *DJI iOSD MARK II Specifications Sheet* [webpage] DJI.com/products/iosd-mark-ii [retrieved 12 May 2016].

APPENDIX

DJI S1000+ Octocopter							
ITEM	WT (lbf)	X-ARM(in)	Y-ARM(in)	Z-ARM (in)	X-MOM	Y-MOM	Z-MOM
Empty Weight	10.20	0.00	0.00	0.00	0.00	0.00	0.00
10000mAh	3.09	0.00	0.00	-5.00	0.00	0.00	-15.45
Empty	0.00	0.00	0.00	0.00	0.00	0.00	0.00
Boom	1.13	0.00	10.63	-10.20	0.00	11.95	-11.48
Sensor 1	0.26	0.30	26.50	-9.45	0.08	6.96	-2.48
Sensor 2	0.26	0.30	34.00	-9.45	0.08	8.93	-2.48
Sensor 3	0.26	0.30	38.00	-9.45	0.08	9.98	-2.48
TOTALS	15.20				0.24	37.81	-34.37
					X-CG Location		0.02
					Y-CG Location		2.49
					Z-CG Location		-2.26

ITEM	WEIGHT
10000mAh	3.09
12000mAh	3.57
16000mAh	4.26
22000mAh	5.50
Boom	1.13
Empty	0.00
FLIR Equip Install	4.13
Sensor 1	0.26
Sensor 2	0.26
Sensor 3	0.26

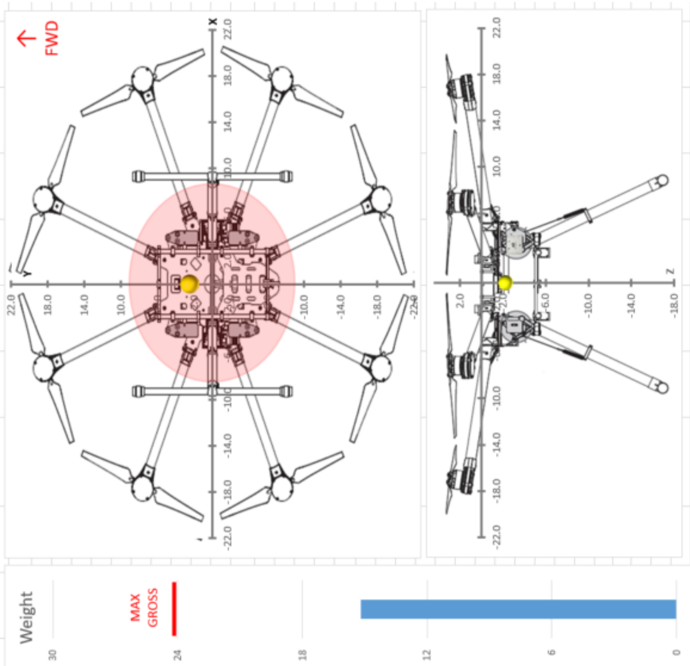

Figure 23 Weight and Balance Calculation Spreadsheet

VITA

Captain Jonathan Lemieux was born in St-Lambert-de-Lauzon, Quebec, Canada, as the third of four children. Upon high school graduation from Stanstead College in Stanstead, Quebec, he enrolled in the Regular Officer Training Program of the Canadian Armed Forces. He attended the Collège Militaire Royal de St-Jean and Royal Military College of Canada, from which he graduated in 2009 with a Bachelors of Engineering degree in Aeronautical Engineering. After obtaining his Aerospace Engineering Officer qualification from the Canadian Forces School of Aerospace Technology and Engineering in 2010, he was posted to the 408 Tactical Helicopter Squadron in Edmonton, Alberta, as the Maintenance Operations Officer for their CH-146 Griffon helicopter fleet. In 2012, he was posted to Cold Lake, Alberta, to the 417 Combat Support Squadron which also operates the CH-146. There, he led the aircraft maintenance team as the Senior Aircraft Maintenance Engineering Officer. In 2014, Captain Lemieux was selected by the Canadian Forces Post Graduate Training Program to complete a degree in Aerospace Engineering at the University of Tennessee Space Institute in Tullahoma, Tennessee. In May 2016, he graduated with a Masters of Science degree in Aerospace Engineering and in November of the same year, with a Masters of Science degree in Engineering Science, Flight Testing. Captain Lemieux then returned to Gatineau, Quebec, to continue his military service as an

Aerospace Engineer under the Director General Aerospace Equipment Program Management.